

Absorption and hot electron production by high intensity femtosecond uv-laser pulses in solid targets

U. Teubner, I. Uschmann, P. Gibbon, D. Altenbernd, and E. Förster

Max-Planck-Arbeitsgruppe "Röntgenoptik" an der Friedrich-Schiller-Universität Jena, Max-Wien-Platz 1, 07743 Jena, Germany

T. Feuerer, W. Theobald, and R. Sauerbrey

Institut für Optik und Quantenelektronik, Friedrich-Schiller-Universität Jena, Max-Wien-Platz 1, 07743 Jena, Germany

G. Hirst, M. H. Key, J. Lister, and D. Neely

Rutherford Appleton Laboratory, Chilton, Didcot, Oxon, OX11 0QX, Great Britain

(Received 6 June 1996)

The interaction of femtosecond KrF*-laser pulses with plasmas of various solid target materials has been studied up to intensities exceeding 10^{18} W/cm². Absorption measurements were performed for *p*- and *s*-polarized laser light and as a function of the laser intensity and the angle of incidence. They reveal substantial absorption up to 70% even at intensities in excess of 10^{18} W/cm². The results have also been compared to simulations of the absorption at high intensities and, in particular, the peaking of the absorption for large angles of incidence (70° – 80°) appears to be consistent with the anomalous skin effect as an important contribution to the total laser pulse absorption. X-ray spectra were measured in the keV range (i.e., between 6.5 and 8.4 Å) and in the soft-x-ray region (i.e., between 25 and 400 Å). The electron density and temperature of the plasma has been estimated by comparison of the experimental spectra with spectral simulations. A systematic study of the hot electrons produced by 248-nm light is presented. Targets consisting of an Al layer on a Si substrate have been used to determine the hot electron yield and the corresponding energy. The *K*- α line emission produced by the hot electrons has been observed as a function of the Al-layer thickness. The measurements have been compared to simulations. The estimated hot electron temperature ~ 8 keV is considerably lower than that deduced from experiments using lasers of longer wavelength and comparable intensities. Scaling indicates that 0.25- μ m lasers can simultaneously fulfill the requirements for both intensity and hot electron temperature for the "fast ignitor." [S1063-651X(96)08610-2]

PACS number(s): 52.40.Nk, 52.25.Nr, 52.50.Jm, 32.30.Rj

I. INTRODUCTION

The interaction of high-intensity laser pulses with matter is an important means of studying the physics of high-temperature laser plasmas [1]. During the past two decades high-energy laser systems with nanosecond laser pulses have been used for plasma production and many studies have been performed related to inertial confinement fusion (ICF) [2]. More recently the development of high-power laser systems with much lower laser energy but ultrashort pulse durations (see, for example, [3,4]) has created an opportunity to generate plasmas under unique conditions, i.e., very high electron densities and very short scale lengths [5,6].

One of the most exciting ideas that has been proposed in connection with the interaction of high-intensity ultrashort laser pulses with matter is the so-called *fast ignitor concept*. Originally proposed by Tabak *et al.* [7], the basic idea of this scheme is to separate fuel ignition from the compression phase, thus lowering the requirements for inertial confinement fusion dramatically. Briefly, after fuel compression the ignition of the core could be performed by a burst of high-energy electrons that will heat the target to the necessary temperature. However, in order to exploit this means of ignition in a controlled way, electrons have to be generated with high efficiency. Furthermore, the electron energy has to be optimized. This means that although the energy has to be

high enough to ignite the fuel, the electrons should not penetrate through the fuel.

In principle, such suprathermal electrons can be generated and accelerated by collisionless absorption [8,9] of an intense ultrashort laser pulse. To achieve a good coupling of the laser light with the plasma and into suprathermal electrons the laser pulse absorption has to be characterized and optimized.

Several experiments of laser pulse absorption [4,5,10–12] and hot electron production [1,13–17] have been performed with infrared high-intensity subpicosecond laser pulses. However, in the context of the fast ignitor it may be of interest to use shorter laser wavelengths (for instance, UV light), because in this case the laser pulse could propagate to higher electron density, i.e., closer to the compressed core, than a pulse of longer wavelength. In addition, from $I\lambda^2$ scaling laws for the hot electron energy [18], it may be estimated that with shorter laser wavelengths the necessary hot electron flux and the optimized energy might be achieved more readily.

Up to now absorption measurements of ultrashort UV-laser pulses have been reported for intensities up to 10^{17} W/cm² [19–22]. However, to our knowledge hot electron generation by such laser pulses have not yet been studied and absorption measurements at the much higher intensities presently accessible are not available.

In this paper the results of the investigation of laser pulse

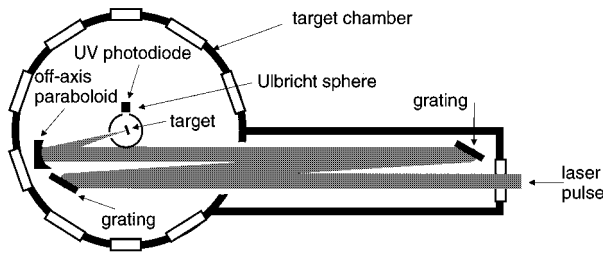


FIG. 1. Experimental arrangement (top view on the grating compressor, the target chamber and the diagnostics for the absorption measurements; for the x-ray measurements the Ulbricht sphere was replaced by the x-ray diagnostics described in the text).

absorption and hot electron production for 380 fs UV-laser pulses and maximum intensities exceeding 10^{18} W/cm² will be presented and discussed. Using the SPRITE KrF*-laser system at the Daresbury Rutherford Appleton Laboratory the absorption has been studied for various experimental conditions, such as different angles of incidence, *s* and *p* polarization, and different laser intensities. The results are presented in Sec. III.

The plasma parameters have been deduced from the experimental x-ray spectra. Section IV is related to these parameters and to the suprathermal electrons. Using the established technique of layered targets [13,15,16] with a *K*- α fluorescer to indicate the penetration depth and intensity of the hot electrons, the conversion efficiency and the average energy has been determined.

II. EXPERIMENTAL ARRANGEMENT

The experiments were carried out using the chirped pulse amplification SPRITE laser system [23] at the Daresbury Rutherford Appleton Laboratory. The experimental scheme is shown in Fig. 1. The laser system delivered approximately 1.7 J pulses at a wavelength $\lambda = 248.5$ nm. The repetition rate was 1 shot every 10–20 min. The energy was monitored for each shot and the shot-to-shot fluctuation was 25%. The pulse duration was 380 fs assuming a Gaussian profile [full width at half maximum (FWHM); with an uncertainty of 20%].

The pulses were focused onto the target with an off-axis parabola (*f*-number 3.2). The intensity distribution of the laser energy in the focus for a typical shot is displayed in Fig. 2. The average diameter of the central part of the focal spot was $3 \mu\text{m}$ (FWHM; with an uncertainty of 20% and a shot-to-shot fluctuation of 30%) and was 2-times diffraction limited. The central spot contained 30% of the maximum energy E_0 on the target surface. The rest of the energy is distributed in an area of roughly 15–20 μm . The maximum energy of $E_0 \approx 250$ mJ was limited by the damage threshold of the grating compressor in the target chamber.

The beam profile was carefully characterized in two ways: (1) the profile of the unamplified laser beam was measured at the position of the target using an UV microscope together with a CCD camera, and (2) it was measured at full energy in a corresponding plane after the last amplifier and near to the target chamber. Although the characterization of the unamplified laser beam would not be subject to *B*-integral effects in transport or perturbations from the *e*-beam amplifiers

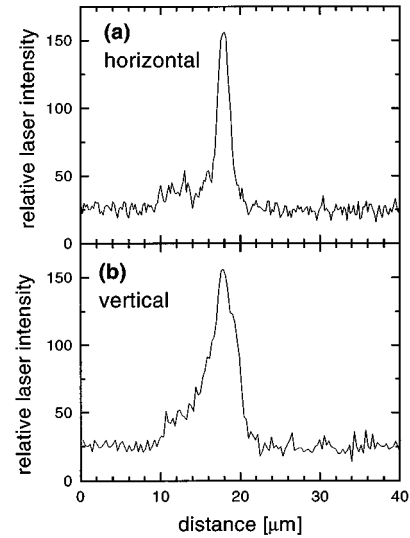


FIG. 2. Intensity distribution of the laser energy in the focus in horizontal (a) and vertical (b) direction.

which the full energy beam might suffer, the equivalent plane measurement actually showed that these effects were small. From both measurements the maximum laser intensity (for normal incidence) $I_{0\perp}$ in the central spot could be estimated to be 5×10^{18} W/cm² with an overall accuracy (systematic error) of 40%.

The amplified spontaneous emission (ASE) from the whole amplifier chain generates a relatively low-intensity prepulse on the target. This intensity is a maximum during the 20 ns period when all three KrF* amplifiers are operating. Its maximum value was estimated by measuring the energy in this period (7 mJ at the target) and dividing it by the pulse duration (20 ns) and the measured spot size (7 μm FWHM). The resulting intensity is about 5×10^{11} W/cm², i.e., an ASE intensity contrast ratio of 10^7 . After some improvements some of the x-ray measurements have been performed also with an about one order of magnitude improved contrast ratio.

The following targets have been used for the experiment: (1) plane highly polished and massive solids of glassy carbon (SIGRADUR), aluminum, silicon, copper, and platinum for the absorption measurements and some of the x-ray measurements and (2) layered targets for most of the other x-ray measurements (vapor deposited aluminum layers of 100, 200, 400, 600, 800, and 1000 nm thickness and foil targets of 1, 1.5, 2, and 6 μm thickness. The substrate of the layered targets was either massive or 10 μm thick silicon). The targets were located in a vacuum chamber and mounted on an *xyz* translation and rotation unit in order to vary the angle of incidence α and to adjust the polarization of the pumping pulse either to the *p* or to the *s* direction with respect to the plane of incidence. Using a high-magnification alignment system the target position was controlled with an accuracy of 10 μm . The targets were moved perpendicular to the laser beam between consecutive shots so that the incident laser beam always struck a fresh spot on the target surface.

The absorption measurements were carried out at three different intensities by changing the energy of the laser beam (the focal spot diameter was always the same): (1) full en-

ergy shots with the whole amplifier chain ($E_0 \approx 250$ mJ), (2) shots with the whole amplifier chain, but now including a dielectric mirror which reduced the energy by one order of magnitude ($E_0 \approx 25$ mJ) and (3) shots using the preamplifier (GOBLIN) only and the final amplifier (SPRITE) switched off ($E_0 \approx 1$ mJ).

The fraction of the absorbed energy was determined by measuring the reflected UV-laser light. This measurement was performed with both a calibrated energy meter and a calibrated Ulbricht sphere which collects all the reflected light except the backreflected fraction. This fraction, however, is less than a few percent and thus negligible [11]. The calibration of the Ulbricht sphere and its linearity were checked before and after the absorption measurements and no significant difference was observed. Interference filters have been used to discriminate between the reflected laser light and the plasma radiation.

The time-integrated x-ray emission of the plasma was measured at various laser intensities, mainly at an angle of incidence of $\alpha = 45^\circ$ and with p -polarized light. The measurements were carried out with an x-ray photodiode and an x-ray pinhole camera ($5 \mu\text{m}$ pinhole and filtered by a $25 \mu\text{m}$ Be-foil). The soft-x-ray region (i.e., between 25 and 400 \AA) was dispersed by a flatfield spectrometer including an aperiodically 1200 lp/mm reflection grating and a cylindrical collection mirror [24] onto an x-ray film (Ilford Q plates). The spectral resolution was between 0.7 and 1.7 \AA .

A ‘‘von Hamos’’ spectrometer [25] with an x-ray film (Kodak DEF) as the detector was used to measure the K - α emission and the x-ray spectra in a wavelength region which could be adjusted in a range between 5 and 8.4 \AA . For each spectrum it was necessary to accumulate between 1 and 5 shots on the film, depending on the laser intensity and the polarization. The spectral resolution $\lambda/\Delta\lambda$ was approximately 1800. Due to the Bragg angle and the aperture of the crystal the observation angle depends on the x-ray wavelength (35.2° for the Si K - α line and 42.4° for the Al K - α line). The observation was from the front side of the Al layers and in a second series from the back side, i.e., behind the Si substrate.

Beside these spectrographs some filter combinations (Al filters of up to 1.02 mm thickness) have been used to detect x-rays up to 20 keV (the detector was a Kodak DEF film) and the hard-x-ray component about 20 keV (with a high sensitive hard-x-ray scintillator behind a 13 mm thick Al plate). The electron temperature of the hot plasma has been estimated from a measurement of the x-ray emission using also various transmission foils of different elements and thicknesses [26]. Here the x-ray detector was again the Kodak DEF film. Finally, and in addition to the x-ray measurements, the current of the ions emitted from the plasma was detected by Faraday cups.

III. LASER PULSE ABSORPTION

A. Experimental results

Figure 3(a) shows the measured total reflectivity as a function of the laser intensity on the target surface I_0 ($I_0 = I_{0\perp} \cos\alpha$). The target was highly polished massive aluminum, the angle of incidence $\alpha = 67^\circ$, and the laser light was p -polarized (R_p , open symbols). The diagram shows

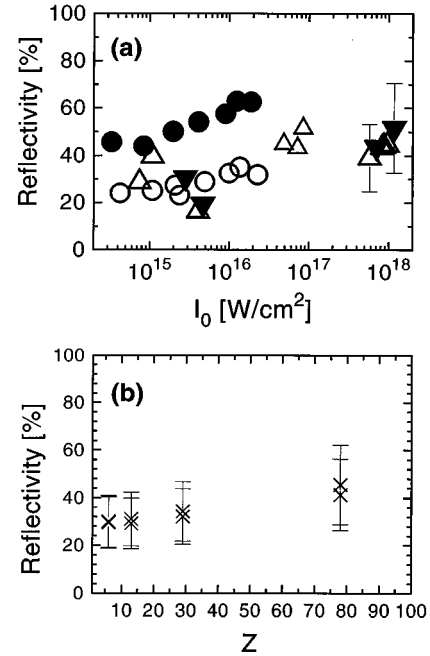


FIG. 3. (a) Intensity dependence (at $\alpha = 67^\circ$) of the reflectivity of 380 fs, 248-nm p -polarized (open symbols) and s -polarized (full symbols) laser pulses. The diagram shows the reflectivity data measured in the present experiment (triangles) and also the data from a previous experiment (circles) [20]. Two typical error bars are included for the statistical error of the individual data points in the present experiment. The systematic error of each reflectivity point is approximately $\Delta R \approx \pm 10\%$ in both experiments. The accuracy of I_0 is about 40%. (b) Dependence (at $\alpha = 67^\circ$) of the reflectivity on the atomic number Z . The measurement was performed with p -polarized light at an intensity of $I_{0\perp} \approx 2.5 \times 10^{18} \text{ W/cm}^2$ and an angle of incidence of $\alpha = 80^\circ$.

the reflectivity data measured in the present experiment (triangles) and also includes the data from a previous experiment (circles) [20]. The systematic error of each reflectivity point is approximately $\Delta R \approx \pm 10\%$ in both the present experiment and also in the previous work. The statistical error of the individual data points may be seen from their fluctuation in the diagram. As mentioned before, the accuracy of I_0 is about 40%.

From Fig. 3(a) it may be seen that the reflectivity for p -polarized laser light, R_p , increases only weakly with the laser intensity from $R_p \approx 25\%$ at $I_0 \approx 10^{14} \text{ W/cm}^2$ to $R_p \approx 45\%$ at $I_0 \approx 10^{18} \text{ W/cm}^2$. The R_p values from the present work and for intensities up to $I_0 \approx 10^{17} \text{ W/cm}^2$ agree with the previous results [20] obtained at lower I_0 but all other experimental conditions are not much different. In addition, the measurements at the lower laser intensities show that nearly all of the light is reflected into the specular direction with a solid angle not much larger than that of the input beam. The angular dependence of the reflectivity [$R_p(\alpha)$, not shown here] has a distinct minimum in the vicinity of $\alpha = 45^\circ$ (at intensities $I_0 \approx 10^{16} \text{ W/cm}^2$) and agrees within the error bars with the previous results [20].

In contrast to the previous lower intensity experiment, at intensities exceeding several times 10^{17} W/cm^2 the non-specular component increases substantially, although the light is still mostly reflected into the specular direction. The

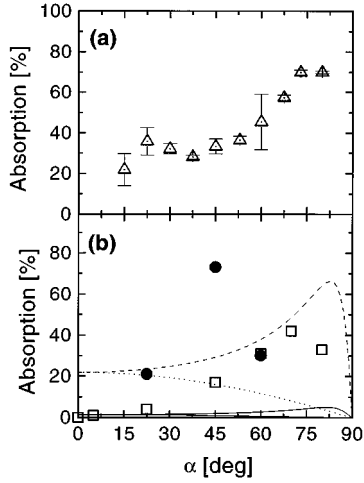


FIG. 4. (a) Angular dependence of the absorption of 380 fs, 248-nm p -polarized laser pulses (at $I_{0\perp} \approx 2.5 \times 10^{18}$ W/cm²; the standard deviation of the intensity of each single shot is 23%). The data points are reproducible and each point is the average of several shots with the statistical error shown as the error bar. The systematic error of all data points together is $\Delta R/R \approx 36\%$. (b) Calculated absorption for obliquely incident light at 10^{18} W/cm² on a step profile from: (i) Fresnel equations with $n_e/n_c = 50$, $T_e = 1$ keV (solid line); (ii) PIC simulation with $n_e/n_c = 10$, $T_e = 1.5$ keV with fixed ions (squares); and (iii) analytical curve for anomalous skin effect with $n_e/n_c = 10$, $T_e = 1.5$ keV; after Ref. [28] (dashed line A_p , dotted line A_s); (iv) PIC simulation with mobile ions; $m_i/m_e = 1836$ (filled circles).

solid angle at 10^{18} W/cm² is roughly a factor of 3 larger than at 10^{16} W/cm² (measured at $\alpha = 45^\circ$). Furthermore, for these higher intensities a shift of the minimum of the $R_p(\alpha)$ curve to larger angles of incidence has been found. This may be seen from Fig. 4(a), where the absorption $A_p = 1 - R_p$ is displayed as a function of α ($I_{0\perp} \approx 2.5 \times 10^{18}$ W/cm²).

The measured reflectivity of s -polarized laser light R_s is lower than expected from the previous lower intensity experiment. From Fig. 3(a) it may be seen that, for instance, at $I_{0\perp} \approx 10^{16}$ W/cm² R_s is lower than measured previously and at intensities exceeding 10^{18} W/cm² the reflectivity and hence also the absorption seems to be the same for p - and s -polarized laser light. However, due to the experimental error a difference of 25% between R_p and R_s cannot be excluded.

Some further reflectivity measurements were performed at $I_{0\perp} \approx 1.5 \times 10^{18}$ W/cm² and $\alpha = 80^\circ$ with p -polarized laser light using various target materials (carbon, aluminum, copper, and platinum, and massive, foil and evaporated targets). It has been found that the reflectivity scales only weakly with the atomic number Z and increases from approximately 30% for light elements ($Z=6$) to nearly 45% for $Z=78$ [Fig. 3(b)]. For Al no significant difference in the reflectivity has been observed between the highly polished massive targets, the foil targets, and the layered targets.

B. Discussion of the absorption results

The reflectivity measurements in Figs. 3(a) and 4(a) imply that the absorption A ($=1 - R$) for the higher intensities

used (10^{18} W/cm²) exhibits a Fresnel-type angular dependence with a maximum at $\alpha = 70$ – 80° . Such behavior is predicted for collisional absorption (inverse Bremsstrahlung) in a highly overdense step profile [19], but for temperatures of the order of 1 keV this contribution is almost negligible [5,27]. Collisionless absorption via the anomalous skin effect also shows a maximum at large angles [28,29]. These two contributions are displayed in Fig. 4(b) for parameters (see Sec. IV) relevant to the experiment, along with results obtained using a particle-in-cell (PIC) code.

For the step profile, in which $L/\lambda = 0$ and the ions remain stationary, this is qualitative agreement between the reflectivity measurements, theory, and PIC simulations. However, further simulations including ion motion and realistic pulse shapes [filled circles in Fig. 4(b)] indicate that the absorption maximum should shift back to 40 – 50° due to the formation of an underdense plasma shelf in front of the target [30]. Relaxation of the density scale length by the prepulse would also shift the absorption maximum towards smaller angles. This would imply that the density gradient remains very steep throughout the interaction with the main pulse, and that ion motion is somewhat inhibited in the present experiment. The reason for this may be the strong ponderomotive force (see Sec. IV B). We conclude that although the theoretical analysis is preliminary, the reflectivity results for p light appear to be consistent with anomalous skin heating in a step-like density profile.

For the reflectivity of s -polarized laser light, R_s , a discrepancy is found and in particular at the highest laser intensity it may be seen [Fig. 4(a)] that $R_s \approx R_p$. This may be explained by the ASE contrast ratio, which leads to a prepulse with an intensity of some 10^{11} W/cm² (at $I_0 \approx 10^{18}$ W/cm²). For s -polarized laser light the ponderomotive force is less efficient and the preplasma may enhance the absorption of the main pulse and thus reduce the reflectivity and, in particular, because this polarization is even more sensitive to the surface conditions than p -polarized laser light [20]. The preplasma effect would also explain the discrepancy between the present results at 10^{16} W/cm² and with preplasma (at this lower intensity the ponderomotive force is also less efficient) and the previous results measured with no preplasma [20].

The increase of the nonspecular part of the reflectivity at high intensities may also be explained by the presence of the preplasma that is created by both, the leading edge of the main laser pulse (at these high intensities the plasma formation threshold is exceeded about 1 ps before the peak of the laser pulse) and the ASE: when the main part of the laser energy hits the preplasma it can be reflected with a much wider angular distribution than from the flat undistributed original target surface.

Other effects which can flatten the angular dependence are surface rippling and hole boring [31]. Assuming the ponderomotive force of the laser exceeds the plasma pressure (compare to Ref. [27]), the critical surface will be pushed inwards at the center of the focal spot, forming a hole the depth h (in μm) given by

$$h \approx \left(\frac{Z}{A}\right)^{1/2} \left(\frac{n_c}{n_e}\right)^{1/2} \left(\frac{t_p}{200 \text{ fs}}\right) a_0,$$

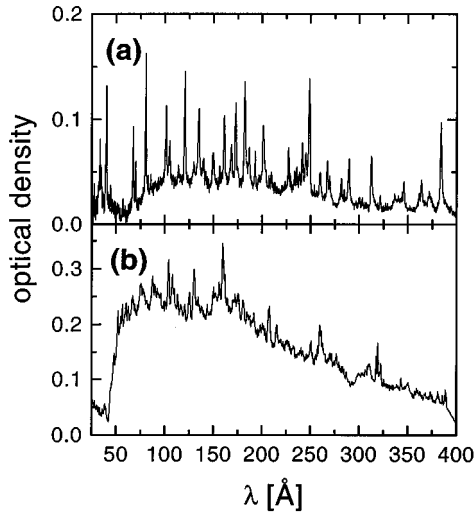


FIG. 5. Microdensitometer scans of two typical soft-x-ray spectra from a carbon plasma (a) and an aluminum plasma (b). The spectra are time- and space-integrated and corrected for background radiation and were measured at an average intensity of 10^{18} W/cm², at $\alpha=45^\circ$ and with p -polarized light pulses. Five laser shots were accumulated for each spectrum.

where A is the atomic number, a_0 the normalized quiver momentum p_{osc}/mc , n_e and n_c are the electron and critical density, respectively, and t_p is the pulse length in fs. For the parameters of interest here, we have $A/Z \approx 2$, $a_0 = 0.3$, $n_e/n_c \approx 10$, and $t_p = 400$ fs, which gives a depth $h \approx 0.13$ μm , or around 1/20 of the spot size. Assuming the hole formed acts as a spherical mirror, this will lead to an additional divergence of 10° , consistent with the observed increase in the nonspecular reflectivity. However, the effect is not strong enough on its own to account for the high absorption seen with s -polarized light. We also note that a more realistic (two-dimensional) analysis would have to take into account the radial intensity distribution of the focal spot, as we consider later for the temperature calculation in Sec. IV F.

IV. X-RAY MEASUREMENTS

A. Soft-x-ray spectroscopy of the hot plasma

Figure 5(a) shows a time integrated carbon spectrum. The observed line emission is due to the radiation from H-like, He-like, Li-like, and a small amount from Be-like carbon ions. The spectrum is dominated by three lines in first and higher orders (up to the eighth order). The identified lines are, namely, the Ly- α , Ly- β , He- α , and He- β lines. Although lines from higher transitions of the H-like ions might be present as well they are not distinguishable from noise. The strongest line in the spectrum is the He- α line, indicating that an appreciable amount of He-like ions are present in the plasma. From the Inglis-Teller limit [32] of the H-like and He-like ions the upper limit of the electron density can be estimated for emission volume of the resonance lines to be less than $(5-10) \times 10^{22}/\text{cm}^3$, i.e., less than 3–6 times the critical electron density n_c ($n_c = 1.8 \times 10^{22}$ cm⁻³ for KrF*-laser radiation).

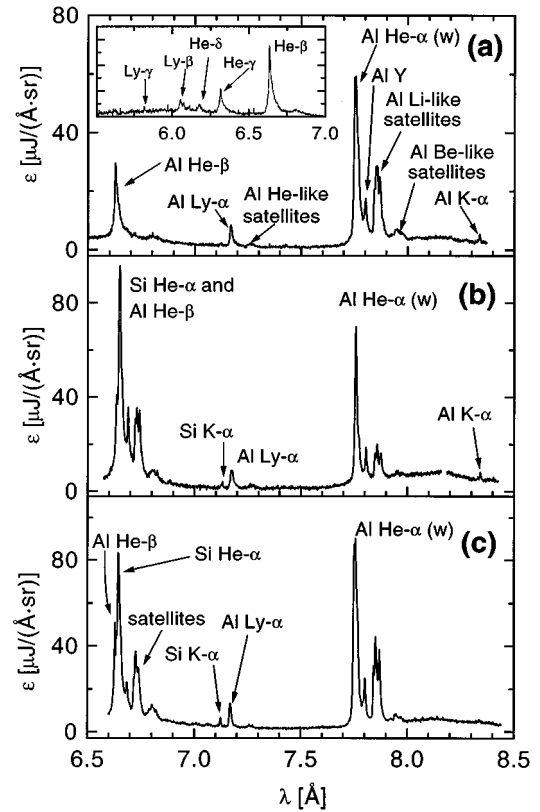


FIG. 6. Von Hamos spectrum observed from a target consisting of a $d=1000$ nm (a), a 600 nm (b) and a 100 nm (c) Al layer on a Si substrate (frontside observation). The spectra were measured with p -polarized light at $I_0=3 \times 10^{18}$ W/cm² and $\alpha=45^\circ$. The ASE intensity contrast ratio was 10^7 . 3–5 shots have been accumulated for each spectrum. The x-ray emission ε is normalized to 1 shot and the background is subtracted. The insert of (a) shows the spectrum at short wavelengths. Lines of H-like ions have been observed up to the Ly- δ line. However, lines from even higher transitions might be present but not be distinguishable from noise.

Similar to before Fig. 5(b) shows a soft-x-ray spectrum recorded with the same experimental conditions but now the target material was Al. The observed lines originate mainly from L -shell transitions. The strongest line in the spectrum can be associated with the Al IV $3s-3p$ transition at 160.1 Å. From Fig. 5 it may be seen that the soft-x-ray emission is of the same order of magnitude for both materials.

B. keV x-ray spectroscopy of the hot plasma

Figure 6(a) shows a K -shell spectrum observed with the von Håmos spectrograph from the front side of a 1000 nm Al layer on a Si substrate. The spectrum was measured with p -polarized light at $I_0=3 \times 10^{18}$ W/cm² and $\alpha=45^\circ$. The spectrum consists of the Al K -shell lines, i.e., the H-like and the He-like resonance lines together with their satellites which are labeled according to the notation of Gabriel [33]. Self-absorption (due to opacity) in the peaks of the He- α and He- β resonance lines has been observed (Fig. 7). The doublet in the Ly- α resonance can be resolved (insert in Fig. 7) and the intercombination line may be clearly seen. Weak continuum emission has been observed as the background of

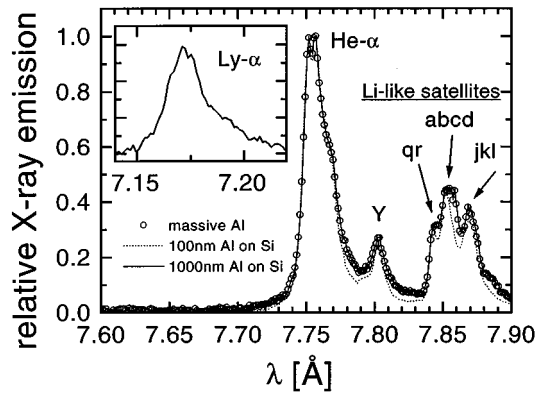


FIG. 7. Spectral shape of the Al He- α group measured with p -polarized light at $I_0=2\times 10^{18}$ W/cm 2 , $\alpha=45^\circ$ and observed from the frontside. All spectra have been normalized to the maximum of the He- α resonance line. The influence of the layer thickness is shown for a spectrum from a massive Al target (circles) and layered targets with a $d=100$ nm (dotted line) and $d=1000$ nm (solid line). The ASE intensity contrast ratio was 10^7 . The insert shows the Ly- α line from a massive Al target.

the spectrum. The “cold” K - α line of the solid Al (i.e., Al I) may be seen as well in this spectrum but no Si K - α emission.

Similarly, Figs. 6(b) and 6(c) show spectra from targets consisting of a 600 and 100 nm Al layer on the Si substrate, respectively. With decreasing layer thickness d the Al I-V (i.e., Al $^{+0\cdots+4}$) K - α line decreases whereas at the same time the Si I-VI (i.e., Si $^{+0\cdots+5}$) K - α line is enhanced. In comparison to similar experiments performed at longer laser wavelength [15–17] the K - α emission from Al and Si is relatively weak if compared to the emission from the hot plasma (e.g., the He- α line). Furthermore, no K - α emission from multiply ionized atoms (i.e., Al V, Al VI, etc.) has been observed within the present experiments.

For $d < 800$ nm [Fig. 6(b) and Fig. 6(c)] x-ray emission from a Si plasma has been observed, i.e., the Si He- α line together with the satellites. Thus a layer of 700–800 nm may be regarded as the time-averaged thickness of the hot plasma. The influence of the Al layer thickness (0.1, . . . , 6 μ m and massive Al targets) on the spectral shape and hence on the plasma conditions is very small and as an example Fig. 7 shows the shape of the He- α group for a massive Al target ($d=\infty$) and layered targets with $d=1\mu$ m and $d=100$ nm Al on Si, respectively. The difference in the spectral shape in this line group is negligible and also the Ly- α group and the He- β line in the corresponding spectra have the same shape. For $d=100$ nm no cold Al K - α emission has been observed. This indicates that most of the Al atoms have been ionized.

The main influence of the shot-to-shot intensity fluctuation on the x-ray emission is that this fluctuation leads to spectra which typically differ by a factor 1–3 in their *strength* but the *shape* of the spectra is reproducible (Fig. 7). This observation agrees with previous measurements where it has been shown that the x-ray emission scales with $(I_0)^{1\cdots 2}$ [10,20,27,34] whereas for instance the electron temperature and the electron density are much weaker functions on I_0 (e.g., T_e scales roughly with the square root of I_0 [10,17,27] and the electron density in the highly ionized

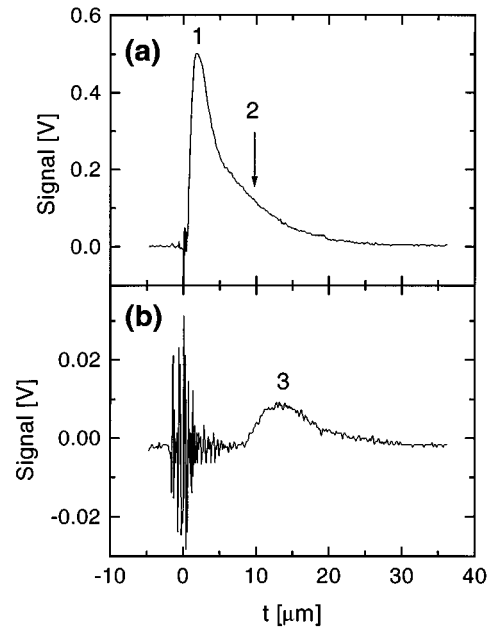


FIG. 8. Time of flight spectra of Al ions from plasmas produced by a full energy shot ($I_0=2\times 10^{18}$ W/cm 2) (a) and by the ASE prepulse only (fs-seed pulse blocked) (b), respectively. The signal was measured with a Faraday cup biased with -70 V and mounted in a distance of 20 cm from the target surface. The angle of observation was 40° . The laser light was p -polarized and the angle of incidence was $\alpha=45^\circ$. The ASE intensity was 5×10^{10} W/cm 2 for both curves. The labeled peaks correspond to ion velocities of 1.2×10^7 cm/s (1), 10^6 cm/s (2) and (3).

plasma depends even less on the laser intensity [34]).

The electron density of the hot Al plasma has been estimated using the x-ray line diagnosis procedures described in [34], i.e., the intensity ratio different satellite lines in the spectra, the width of the resonance lines (Ly- α , He- α , and He- β) and in addition the intensity ratio of the lines in the Ly- α resonance doublet [35]. From these diagnostics an electron density n_e of 1–2 times the critical density may be estimated for the emission volume of the resonance lines whereas the emission from the satellites originates from even higher densities ($n_e > 4n_c$).

Finally, it should be mentioned that there was no signal of x rays exceeding 10 keV photon energy.

C. Ion measurements

The influence of the ASE prepulse was surveyed by blocking the fs-seed pulse. By observation of the ion signals from the Faraday cups [36] an onset of plasma production has been found at both the lower and the improved contrast ratio. As an example Fig. 8 shows the time-of-flight spectra of an Al plasma produced by a full energy shot (a) and a plasma produced by only ASE (b), respectively. The temporal zero point is assumed to coincide with the electromagnetic noise signal from the laser discharge. The peaks in Figs. 8(a) and 8(b) correspond to ions with velocities of 1.2×10^7 cm/s (1) and 10^6 cm/s (3) (fast ions with velocities exceeding 10^8 cm/s could not be distinguished from the noise signal).

Peak 1 can be explained by the thermal expansion of the hot plasma. In addition, it has been found that the ion velocity is nearly the same for both contrast ratios and independent of the target material (i.e., Al, Si or layered targets), but the signal height depends strongly on the contrast ratio and differs by a factor of 2–6 between “low” and “high” contrast ratio. In contrast to the measurements of Meyerhofer *et al.* [10] it has been observed that the signal increases with the prepulse intensity. Using a convenient model for the plasma expansion [37] a lower limit for the electron temperature may be estimated from this peak to be of the order of 300–400 eV (this value corresponds to the expanded plasma which is collisionless [38]). Peak 3 arises from the preplasma and it may be seen that a similar peak (2) is covered in the wing of the time-of-flight signal in Fig. 8(a). These peaks correspond to an electron temperature of the preplasma of 8 eV.

However, the effect of the prepulse on the generation of the *x-ray emission from the hot plasma* is not too strong. This may be seen from both the Faraday cup measurements (see above) and from the comparison of the Al spectra from the present work with those measured at one order of magnitude less intensity but better contrast ratio [34]. The shape of the line emission in both experiments is nearly the same and thus indicates that also the electron density is not much different.

The reason for this may be the following. Although it is expected that the ASE prepulse leads in principle to a lower density plasma this may be partly compensated by the ponderomotive force at high laser intensities which strongly pushes the plasma at the critical density [17,27,34,39]. Thus the x-ray emission and the energy deposition still take place in the overdense region.

D. Electron temperature of the hot plasma

The time averaged electron temperature *of the hot plasma* \bar{T}_e has been estimated from the foil transmission measurements. For the aluminum plasmas produced by an intensity of $I_0 = 10^{18}$ W/cm² and *p*-polarized laser light at $\alpha = 45^\circ$ \bar{T}_e is approximately 1500 eV with a systematic error of 500 eV. This value agrees with the $\bar{T}_e(I_0)$ dependence deduced previously for Al subpicosecond UV laser produced plasmas [27,34]. The electron temperatures \bar{T}_e of the Si plasmas and the plasmas from the massive and layered Al targets produced with nearly the same experimental conditions are approximately the same and thus indicate similar plasma conditions for both materials.

Obviously, \bar{T}_e is much lower than the “initial temperature” $T_{e,o}$, i.e., the temperature at the peak of the laser pulse, which can be estimated [27] for the present experimental conditions to exceed $T_{e,o} \approx 3$ keV (in the vicinity of the critical density). Similar to the hot electron temperature deduced from the high energetic electrons, i.e., T_h (this will be discussed in the following section) this temperature corresponds to a temporal snapshot, however, from a differential spatial region ($T_{e,o}$: from the hot plasma; T_h : from electrons which are accelerated into the bulk material, where most of the *K*- α line radiation occurs).

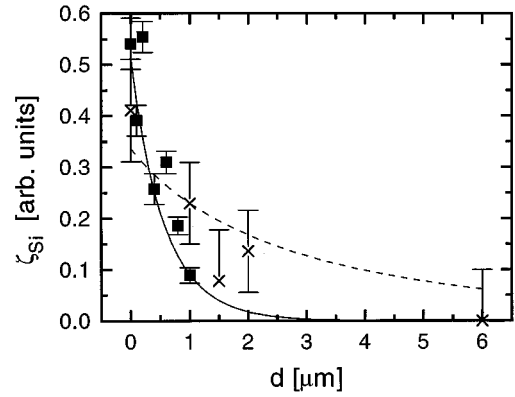


FIG. 9. Si *K*- α line intensity ζ emitted from Al layered targets on a Si substrate and observed from both, front side (closed square symbols) and back side (cross symbols) as a function of Al layer thickness d . The incident laser intensity was 10^{18} W/cm², the angle of incidence 45° and the light was *p*-polarized. All data have been corrected for reabsorption in the Al and Si layers, respectively, and in addition, they have been normalized to the accumulated incident laser energy. The result of the simulation using a hot electron temperature of $T_h = 8$ keV is shown for both the front-side (solid line) and back-side (dashed line) observation.

E. Energy of the fast electrons

The measurement of the *K*- α emission in multilayered targets is a well established method [13,15,16] to study the energy of the hot electrons. In the present experiments these electrons were produced near the target surface in a region not larger than several hundred nanometers thickness (see Sec. IV B) and at densities close to the critical density.

The basic idea to determine the energy of the hot electrons (i.e., the so-called *hot electron temperature* T_h) is that they lose part of their kinetic energy in the Al layer before they penetrate into the Si substrate. In both materials those electrons which still have enough energy (exceeding the *K*-shell binding energy) can ionize the cold atoms and thus lead to *K*- α emission from the Al and Si atoms. Thus, varying the thickness of the Al layers affects the absolute value and the ratio of the Al and Si *K*- α line intensity. Hence a measurement of the line intensity ratio as a function of layer thickness (e.g., see Figs. 6 and 9) provides a method for deducing the penetration depth of the hot electrons and thus the electron energy.

To our knowledge all previous experiments which have used this method detected the *K*- α emission from the front side of the target surface, which means that the emission from the substrate material had to penetrate the layer on the target surface. By contrast, back-side observation has advantages: reabsorption of the *K*- α line in the substrate material is relatively low because of the lack of the *K* shell for photoelectric absorption. Thus the *K*- α line emission may be observed quite efficiently from the back side if the thickness of the substrate does not exceed a value of the order of $1/\mu$ (μ is the photoelectric absorption coefficient). This corresponds to a maximum thickness for the substrate of 9.5 μm for aluminum and 12.3 μm for silicon.

The advantage arises from the possibility to excite the *K* states of Al by the emitted Si *K*- α line. Due to the lower energy Al *K*- α emission cannot lead to the excitation of the

K state of silicon. However, Si K - α emission can in principle excite the Al K states and thus influence the relative ratio of both lines. Thus, in the case of front-side observation where the Si K - α emission has to propagate through the Al layer the absorption depth of about $1.1 \mu\text{m}$ gives a limitation of the precision of the electron energy determination.

Before the hot electron temperature was calculated the artificial contribution of the K -shell excitation by x-ray photons emitted from the hot plasma has been estimated by taking into account all spectral components of the hot plasma which could excite the K shell. However, it has been found that such K - α fluorescence is not of much importance, in particular, for thick Al layers.

In order to extract T_h from the dependence of the K - α signals on the layer thickness a simple model has been developed and the experimental data were compared with the simulation. The one-dimensional model is based on the assumption of the Bethe-Bloch energy loss function dE_e/dx (E_e is the electron energy) and neglects elastic scattering of the electrons. As a first approximation the electron energy distribution, which cannot be determined from the experiment, is assumed to be Maxwellian. Later we consider distributions calculated from PIC simulations (Sec. IV F). With these assumptions the energy fraction $F(E_e)$ converted into K - α radiation is

$$F(E_e) = \frac{n_A \sigma_K(E_e) E_K}{\frac{dE_e}{dx}}, \quad (1)$$

where n_A is the number of atoms per unit volume, σ_K the cross section for K -shell impact ionization (taken from [40]), and E_K the energy necessary to ionize the K shell. The K - α yield per electron and solid angle is given by

$$\zeta(E_e) dE_e = \frac{1}{4\pi} \frac{E_{K\alpha}}{E_K} \eta_K F(E_e) dE_e, \quad (2)$$

with the energy $E_{K\alpha}$ of one K - α photon and the fluorescence efficiency η_K . Now the total yield may be obtained by integrating over the whole energy range

$$\zeta(T_h) = \int_0^\infty \zeta(E_e) f(E_e, T_h) dE_e, \quad (3)$$

where $f(E_e, T_h)$ is the Maxwell-Boltzmann distribution function (this turns out to be a reasonable assumption when compared to self-consistently calculated energy distributions from the PIC simulation; see Sec. IV F).

The result of the calculation may be seen in Fig. 9, where the Si K - α yield ζ_{Si} observed from both front side and back side is plotted as a function of layer thickness d . All data have been corrected for reabsorption in the Al and Si layers, respectively, using the absorption coefficients from Ref. [41]. In addition, due to the shot-to-shot fluctuation of the laser energy and the accumulation of several shots for some of the spectra the data have been normalized to the accumulated incident laser energy.

The hot electron temperature has been fitted for both front-side and back-side observation and as expected (see above) it was found that the detection from the back side is

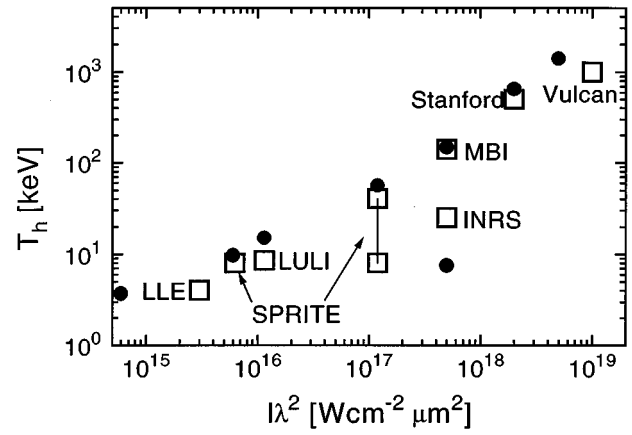


FIG. 10. Comparison of the hot electron temperatures deduced from various experiments (open squares): LLE is from Ref. [15] ($\alpha=60^\circ$, p -pol.), LULI from Ref. [16] ($\alpha=7^\circ$, p -pol.), SPRITE from the present work ($\alpha=45^\circ$, p -pol.), INRS from Ref. [17] ($\alpha=0^\circ$, s -pol.), MBI from Ref. [11] ($\alpha=45^\circ$, p -pol.), Stanford from Ref. [14] ($\alpha=30^\circ$, p -pol.), Vulcan from Ref. [1] (p -pol.). The corresponding points calculated by PIC simulations with the same conditions are shown as well (solid circles). The two points of the present work correspond to the two intensities of the ‘‘double-box’’ energy distribution described in the text.

more sensitive. The best fit of the experimental data was obtained with $T_h=8$ keV (Fig. 9). This temperature may be regarded as a lower limit because additional consideration of electron scattering in the calculation would give a smaller simulated penetration depth for an electron of the same energy and hence a lower K - α intensity [42].

It should be mentioned that the detection efficiency in the experiment did not permit the high-energy component to be measured more precisely. This was because for thicker layers it would have been necessary to accumulate much more than five shots for a spectrum, which was not possible with the repetition rate of 1 shot every 10–20 min.

F. Discussion

The value of T_h deduced from the K - α measurements is significantly lower than that expected from similar experiments with short pulse lasers assuming the usual scaling [43] with some fractional power of $I\lambda^2$; see Fig. 10. In fact, the value from the present experiment would be consistent with characteristic energies acquired by electrons under s -polarized illumination. In this case, one can naively expect an electron to gain an oscillatory energy normal to the target of

$$U_{\text{osc}} = 511 \frac{(v_{\text{osc}})^2}{4} \cos(\alpha) \text{ keV} \\ = \frac{1}{4} \frac{(2I\lambda^2)}{1.4 \times 10^{18} (1/\sqrt{2})} = 16 \text{ keV}. \quad (4)$$

Since this is a monoenergetic estimate, subsequent thermalization would lead to equivalent (Maxwellian) temperatures of 6–10 keV, consistent with the measured value. On the other hand, the measurements here were made entirely with

p -polarized light, for which much higher temperatures can be expected due to the presence of more efficient heating mechanisms such as resonance absorption [20,22] and vacuum heating [8]. Indeed, PIC simulations with parameters relevant to the present experiment yield quasi-Maxwellian hot electron distributions with temperatures of 40 keV for p -polarized light at $I = 2 \times 10^{18}$ W/cm²; Fig. 10. A complementary simulation with s -polarized light gives a temperature of 5 keV, in agreement with the simple estimate above [Eq. (4)].

The discrepancy can be at least partly explained by taking into account the radial pulse profile, which was far from Gaussian (Fig. 2). As mentioned in Sec. II, only 30% of the total energy was contained in the central ($3 \mu\text{m}$) spot; the remaining 70% was distributed over a much broader area of $15\text{--}20 \mu\text{m}$ diameter. In other words, the hot electrons produced in the wings of the central spot may well dominate the overall $K\text{-}\alpha$ signal. To check this, we can combine the output from two PIC simulations and use the result as input for the stopping calculation (Sec. IV E).

First, we assume a simplified radial profile with a hot spot of diameter $\sigma_0 = 3 \mu\text{m}$ at $I_0 = 2 \times 10^{18}$ W/cm², surrounded by a broader spot with $\sigma_w = 20 \mu\text{m}$ at $I_w = 10^{17}$ W/cm². Since the PIC simulation is 1D, the hot electron distributions $f_h(E_e)$ must be weighted by the total area irradiated by the respective components, that is,

$$\frac{N_w}{N_0} = \frac{\sigma_w^2 f_{hw}}{\sigma_0^2 f_{h0}} = 45 \frac{f_{hw}}{f_{h0}}. \quad (5)$$

The result is depicted in Fig. 11(a), which shows the weighted distributions from two simulations at different intensities together with the sum representing the net distribution for this ‘‘double-box’’ profile.

Next, this distribution is fed into the stopping calculation [Eqs. (1)–(3)], the result of which is shown in Fig. 11(b), along with the result for the 8 keV Maxwellian from Fig. 9. We see immediately that the $K\text{-}\alpha$ ratio is dominated by the colder electrons from the larger, low-intensity spot. A more quantitative comparison using a double distribution is not possible without including elastic scattering.

V. CONCLUSIONS

The interaction of 380 fs KrF*-laser pulses and up to intensities 10^{18} W/cm² has been investigated in detail and, in particular, the present experiments address both the coupling of UV laser radiation at high intensities and the production of fast electrons from the laser-target interaction.

Absorption measurements have been performed as a function of the laser intensity and the angle of incidence for both p - and s -polarized laser light. The absorption measurements reveal substantial absorption of about 60–70 % of the p -polarized laser radiation in the solid even at intensities in excess of 10^{18} W/cm². The peaking of the absorption for p -polarized laser light and large angles of incidence, i.e., $70^\circ\text{--}80^\circ$ are consistent with the anomalous skin effect in a steplike density profile as an important contribution to the total laser pulse absorption [28,29]. Furthermore, this would imply that the preplasma that was present in the experiment is strongly pushed by the ponderomotive pressure due to the

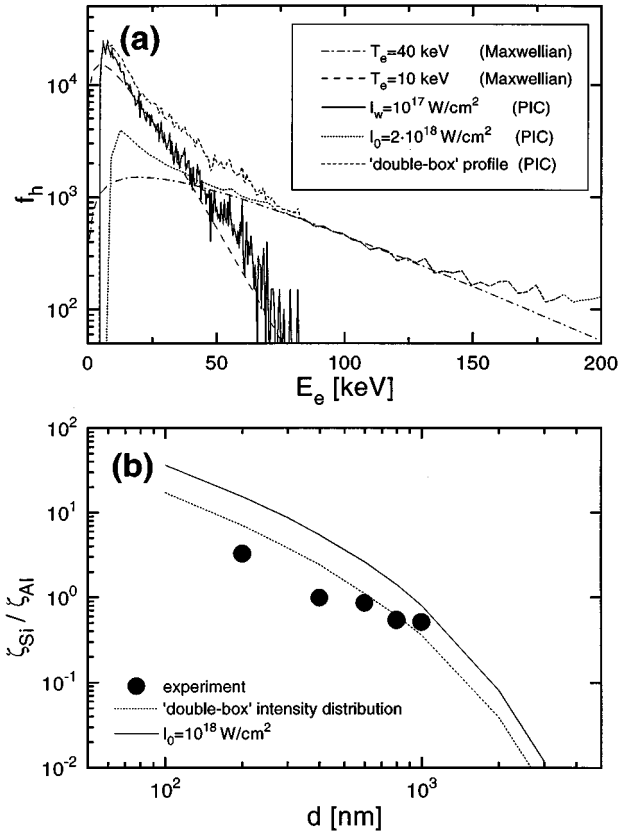


FIG. 11. (a) Weighted distributions from two simulations at different intensities ($I_w = 10^{17}$ W/cm², $\sigma_w = 20 \mu\text{m}$: solid line; $I_0 = 2 \times 10^{18}$ W/cm², $\sigma_0 = 3 \mu\text{m}$: dotted line) together with the sum representing the net distribution for this ‘‘double-box’’ profile (short dash). Maxwellian distributions ($T_e = 10$ keV: dashed line; $T_e = 40$ keV: dot-dashed line) are also shown for comparison. (b) Ratio of the Si $K\text{-}\alpha$ line intensity to that of the Al $K\text{-}\alpha$ line intensity from the experiment (front-side observation; dots) and from the simulation ($I_0 = 2 \times 10^{18}$ W/cm²: solid line; double-box intensity distribution: dotted line) using the distributions shown in (a). The result for $I_w = 10^{17}$ W/cm² is nearly indistinguishable from the result using the double-box intensity distribution.

high laser intensity (in agreement with other experiments [17,34,39]) and thus still lead to a steep electron density profile. By contrast, the ponderomotive pressure for s -polarized laser light is weaker, the radiation is more sensitive to the preplasma and it is less efficiently absorbed, especially at the lower intensities.

X-ray spectra from Al plasmas have been measured in both the keV range and in the soft-x-ray region. Analysis of the spectra indicates that the electron temperature of the hot plasma exceeds 1 keV and the electron density has a value of several times the critical density. From the time-integrated measurements of the spectra it has been shown that the hot plasma does not extend more than several 100 nm behind the original target surface and that a surface layer of 100 nm is fully ionized.

The experiment has also shown that the laser plasma interaction does not depend strongly on the target material if the laser intensity exceeds 10^{18} W/cm². The absorption scales only weakly with the atomic number and it increases from approximately 30% for light elements to 45% for

$Z=78$ (for $\alpha=80^\circ$). In addition, from the x-ray measurements and the detected ion signals it may be deduced that also the plasma parameters are not much different.

The hot electrons produced by 248-nm light have been studied. A systematic investigation of the hot electron yield and the corresponding energy from targets consisting of an Al layer on a Si substrate was carried out. The $K\text{-}\alpha$ line emission produced by the hot electrons has been observed as a function of the Al-layer thickness from both the front side of the target and the back side.

Simulations were performed combining a PIC code with a stopping model based on the Bethe-Bloch energy loss function. A simple comparison of the experiment with PIC simulations shows that the hot electron temperature is considerably lower when compared to visible and infrared laser radiation and comparable intensities if a single laser intensity is assumed in the modeling. However, further investigation shows that it is essential to take into account a more realistic laser intensity distribution in the focal spot. Indeed, the anomalously low measured temperature can be explained by assuming that the contribution of hot electrons from the wings of the focal spot dominates. A simple ‘‘double-box’’ profile gives a good estimate for the hot electron temperature

which is more consistent with that expected from the $I\lambda^2$ scaling: we find $T_h \approx 40$ keV and $T_h \approx (8 \pm 2)$ keV for the two intensities 2×10^{18} W/cm² and 10^{17} W/cm² comprising the whole focal spot.

The requirement for a realistic ‘‘fast ignitor’’ laser have been estimated to 10^{20} W/cm² and a pulse duration of about 10 ps to push the underdense plasma and electrons of ~ 1 MeV are required for ignition. $I\lambda^2$ scaling of 1 μm lasers to 10^{20} W/cm² yields hot electron temperatures well in excess of 10 MeV, too hot for efficient target ignition. The same scaling for 0.25 μm lasers yields hot electron temperatures in the 1 MeV range corresponding to the required electron energies for target ignition.

ACKNOWLEDGMENTS

The authors would like to thank O. Willi for discussions and making his results on laser pulse absorption available for them prior to publication. The authors are grateful to G. Teufer for the careful preparation of the targets. This work was supported (in part) by the Human Capital and Mobility Programme of the European Community.

-
- [1] A. P. Fews, P. A. Norreys, F. N. Beg, A. R. Bell, A. E. Dangor, C. N. Danson, P. Lee, and S. J. Rose, *Phys. Rev. Lett.* **73**, 1801 (1994); B. A. Hammel, F. N. Beg, A. R. Bell, A. E. Dangor, C. B. Darrow, A. P. Fews, M. Glinsky, M. Holden, P. Lee, P. A. Norreys, M. Tafarakis, and G. J. Tallents, in *High Field Interactions and Short Wavelength Generation*, OSA Tech. Dig. Ser. Vol. 16 (Optical Society of America, Washington, D.C., 1994).
- [2] J. Lindl, *Phys. Plasmas* **2**, 3933 (1995).
- [3] T. S. Luk, A. McPherson, G. Gibson, K. Boyer, and C. K. Rhodes, *Opt. Lett.* **14**, 1113 (1989); W. Tighe, C. H. Nam, J. Robinson, and S. Suckewer, *Rev. Sci. Instrum.* **59**, 2235 (1988); G. A. Kyrala, R. D. Fulton, E. K. Wahlin, L. A. Jones, G. T. Schappert, J. A. Cobble, and A. J. Taylor, *Appl. Phys. Lett.* **60**, 2195 (1992); Y. Nabekawa, K. Kondo, N. Sarukura, K. Sajiki, and S. Watanabe, *Opt. Lett.* **18**, 1922 (1993); C. N. Danson, L. J. Barzanti, Z. Chang, A. E. Damerell, C. B. Edwards, S. Hancock, M. H. R. Hutchinson, M. H. Key, S. Luan, R. R. Mahadeo, I. P. Mercer, P. Norreys, D. A. Pebler, D. A. Rodkiss, I. N. Ross, M. A. Smith, R. A. Smith, P. Taday, W. T. Toner, K. W. M. Wigmore, T. B. Winstone, R. W. Wyatt, and F. Zhou, *Opt. Commun.* **103**, 392 (1993); S. Szatmari, *Appl. Phys. B* **58**, 211 (1994); M. D. Perry, and G. Mourou, *Science* **264**, 917 (1994).
- [4] H. M. Milchberg, R. R. Freeman, and S. C. Davey, *Phys. Rev. Lett.* **61**, 2364 (1988).
- [5] J. C. Kieffer, P. Audebert, M. Chaker, H. Pepin, T. W. Johnston, P. Maine, D. Meyerhofer, J. Delettrez, D. Strickland, P. Bado, and G. Mourou, *Phys. Rev. Lett.* **62**, 760 (1989); *IEEE J. Quantum Electron.* **QE-25**, 2640 (1989); M. Chaker, J. C. Kieffer, J. P. Matte, H. Pepin, P. Audebert, P. Maine, D. Strickland, P. Bado, and G. Mourou, *Phys. Fluids B* **3**, 167 (1991).
- [6] O. L. Landen and W. E. Alley, *Phys. Rev. A* **46**, 5089 (1992).
- [7] M. Tabak, J. Hammer, M. E. Glinsky, W. L. Kruer, S. C. Wilks, J. Woodworth, E. M. Campbell, M. D. Perry, and R. J. Mason, *Phys. Plasmas* **1**, 1626 (1994).
- [8] F. Brunel, *Phys. Rev. Lett.* **59**, 52 (1987); P. Gibbon and A. R. Bell, *ibid.* **68**, 1535 (1992).
- [9] T.-Y. B. Yang, W. L. Kruer, R. M. More, and A. B. Langdon, *Phys. Plasmas* **2**, 3146 (1995).
- [10] D. D. Meyerhofer, H. Chen, J. A. Delettrez, B. Soom, S. Uchida, and B. Yaakobi, *Phys. Fluids B* **5**, 2584 (1993).
- [11] M. Schnürer, M. P. Kalashnikov, P. V. Nickles, Th. Schlegel, W. Sandner, N. Demchenko, R. Nolte, and P. Ambrosi, *Phys. Plasmas* **2**, 3106 (1995).
- [12] D. F. Price, R. M. More, R. S. Walling, G. Guethlein, R. L. Shepherd, R. E. Stewart, and W. E. White, *Phys. Rev. Lett.* **75**, 252 (1995).
- [13] J. D. Hares, J. D. Kilkenny, M. H. Key, and J. G. Lunney, *Phys. Rev. Lett.* **42**, 1216 (1979); N. A. Ebrahim, C. Joshi, and H. A. Baldis, *Phys. Rev. A* **25**, 2440 (1982); B. Luther-Davies, A. Perry, and K. A. Nugent, *ibid.* **35**, 4306 (1989); C. Rousseaux, F. Amiranoff, C. Labaune, and G. Matthieussent, *Phys. Fluids B* **4**, 2589 (1992).
- [14] J. D. Kmetec, C. L. Gordon, J. J. Macklin, B. E. Lemoff, G. S. Brown, and S. E. Harris, *Phys. Rev. Lett.* **68**, 1527 (1992).
- [15] H. Chen, B. Soom, B. Yaakobi, S. Uchida, and D. D. Meyerhofer, *Phys. Rev. Lett.* **70**, 3431 (1993).
- [16] A. Rousse, P. Audebert, J. P. Geindre, F. Fallières, J.-C. Gauthier, A. Mysyrowicz, G. Grillon, and A. Antonetti, *Phys. Rev. E* **50**, 2200 (1994).
- [17] Z. Jiang, J. C. Kieffer, J. P. Matte, M. Chaker, O. Peyrusse, D. Gilles, G. Korn, A. Maksimchuk, S. Coe, and G. Mourou, *Phys. Plasmas* **2**, 1702 (1995).
- [18] W. L. Kruer, *The Physics of Laser Plasma Interaction*

- (Addison-Wesley, Redwood City, 1988).
- [19] R. Fedosejevs, R. Ottmann, R. Sigel, G. Kühnle, S. Szatmari, and F. P. Schäfer, *Appl. Phys. B* **50**, 79 (1990); *Phys. Rev. Lett.* **64**, 1250 (1990).
- [20] U. Teubner, J. Bergmann, B. van Wousterghem, F. P. Schäfer, and R. Sauerbrey, *Phys. Rev. Lett.* **70**, 794 (1993).
- [21] D. Riley, L. A. Gizzi, A. J. Mackinnon, S. M. Vianna, and O. Willi, *Phys. Rev. E* **48**, 4855 (1993).
- [22] R. Sauerbrey, J. Fure, S. P. Le Blanc, B. van Wousterghem, U. Teubner, and F. P. Schäfer, *Phys. Plasmas* **1**, 1635 (1994).
- [23] I. N. Ross, A. R. Damerell, E. J. Divall, J. Evans, G. J. Hirst, C. J. Hooker, J. R. Houlston, M. H. Key, J. M. D. Lister, K. Osvay, and M. J. Shaw, *Opt. Commun.* **109**, 288 (1994).
- [24] T. Kita, T. Harada, N. Nakano, and H. Kuroda, *Appl. Opt.* **22**, 512 (1983); D. Neely, A. Damerell, R. Parker, and M. Zepf, Rutherford Appleton Laboratory Annual Report TR-95-025, 1994 (unpublished).
- [25] Details of this spectrometer and the spectrum analyzation have been described in Ref. [34]. The film calibration curve for the present experiments was taken from B. L. Henke, J. Y. Uejio, G. F. Stone, C. H. Dittmore, and F. G. Fujiwara, *J. Opt. Soc. Am. B* **3**, 1540 (1986).
- [26] H. Puell, H. J. Neusser, and W. Kaiser, *Z. Naturforsch. Teil A* **25**, 1815 (1970).
- [27] U. Teubner, P. Gibbon, and E. Förster, F. Fallières, P. Audebert, J. P. Geindre, and J. C. Gauthier, *Phys. Plasmas* **3**, 2679 (1996).
- [28] A. A. Andreev, E. G. Gamalii, V. N. Novikov, A. N. Semakhin, and V. T. Tikhonuk, *Sov. Phys. JETP* **74**, 963 (1992).
- [29] H. Ruhl and P. Mulser, *Phys. Lett. A* **205**, 388 (1995).
- [30] P. Gibbon, *Phys. Rev. Lett.* **73**, 664 (1994).
- [31] S. C. Wilks, W. L. Kruer, M. Tabak, and A. B. Langdon, *Phys. Rev. Lett.* **69**, 1383 (1992).
- [32] J. C. Gauthier, in *Laser-Plasma Interactions 4*, SUSSP Proc. **35**, edited by M. B. Hooper (IOP, Bristol, U.K., 1988).
- [33] A. H. Gabriel, *Mon. Not. R. Astron. Soc.* **160**, 99 (1972).
- [34] U. Teubner, T. Mißalla, I. Uschmann, E. Förster, W. Theobald, and C. Wülker, *Appl. Phys. B* **62**, 213 (1996).
- [35] V. A. Boiko, S. A. Pikuz, and A. Ya. Faenov, *J. Phys. B* **12**, 1889 (1979).
- [36] I. Pelah, *Phys. Lett.* **59A**, 348 (1976).
- [37] S. J. Gitomer, R. D. Jones, F. Begay, A. W. Ehler, J. F. Kephart, and R. Kristal, *Phys. Fluids* **29**, 2679 (1986); Y. Y. Tsui, R. Fedosejevs, and A. A. Offenberger, *Phys. Fluids B* **5**, 3357 (1993).
- [38] D. Salzmann (private communication).
- [39] O. Peyrusse, M. Busquet, J. C. Kieffer, Z. Jiang, and C. Y. Cote, *Phys. Rev. Lett.* **75**, 3862 (1995).
- [40] W. Lotz, *Z. Phys. (Leipzig)* **232**, 101 (1969).
- [41] B. L. Henke, P. Lee, T. J. Tanaka, R. L. Shimabukuro, and B. K. Fujikawa, *At. Data Nucl. Data Tables* **27**, 1 (1982).
- [42] Self-consistent inclusion of elastic scattering using a Monte-Carlo method leads to inferred temperatures between 50 and 100 % higher than those from the simple stopping calculation; A. Rousse (private communication).
- [43] D. W. Forslund, J. M. Kindel, K. Lee, and *Phys. Rev. Lett.* **39**, 284 (1977).